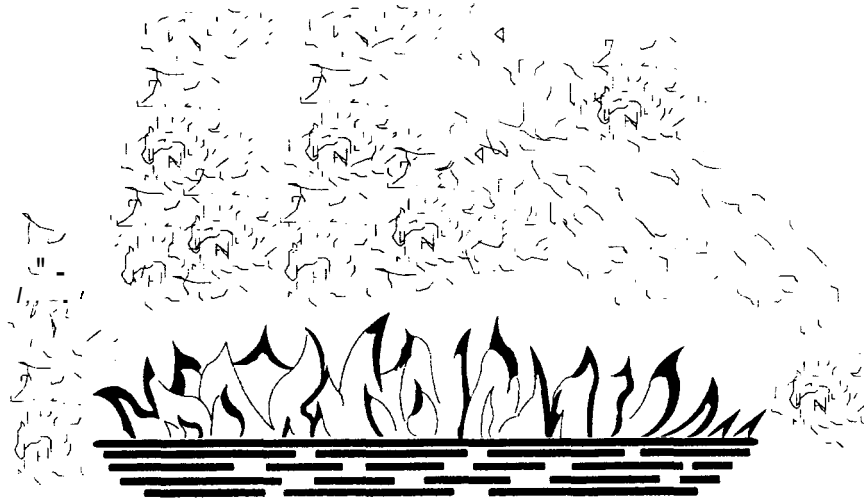


**Appendix A: Benchmark Analysis with FLAMME–S,
Eric BOUTON, and Bruno TOURNIAIRE, IPSN, France**



INSTITUT DE PROTECTION ET DE SURETE NUCLEAIRE

DEPARTEMENT DE RECHERCHES EN SECURITE



	REDACTION E. BOUTON	VERIFICATION	ING. AQ.	APPROBATION
NOM	B. TOURNIAIRE	C. CASSELMAN	P. SOUSSAN	R. GONZALEZ
DATE				
VISA				
REV. A				
REV. B				
Titre	Study of cable tray fires of redundant safety trains with the Flamme_S code.			
Auteur(s)	E. BOUTON - B. TOURNIAIRE			
Type Rapport			Numero SESHP/GME/IPS/FLS/C60/RP/00.930	

La diffusion des informations contenues dans ce document auprès d'un tiers extérieur au CEA est soumise à l'accord de l'unité émettrice de l'IPSN.

This document, which contains proprietary or other confidential or privileged information, and any reproduction in whole or in part, shall not be disseminated outside the organization of the recipient without prior approval of the IPSN.

IPSN/DRS/SESHP/GMEF

Cadarache, le 06/10/00

Rapport - SESHP/GME/IPS/FLS/C60/RP/00.930

**Study of cable tray fires of redundant safety trains with the
Flamme_S code.**

E. BOUTON - B. TOURNIAIRE

*La diffusion des informations contenues dans ce document auprès d'un tiers extérieur au CEA est soumise à l'accord de
l'unité émettrice de l'IPSN.*

*This document, which contains proprietary or other confidential or privileged information, and any reproduction in whole
or in part, shall not be disseminated outside the organization of the recipient without prior approval of the IPSN.*



SERVICE D'ESSAIS DE SURETE HORS PILE		
Groupe Modelisation et Etudes des Feux		
Vat. Document	Rapport	
TITRE	Study of cable tray fires of redundant safety trains with the Flamme_S code.	
Auteur(s)	E. BOUTON - B. TOURNIAIRE	
Type de diffusion : Normale	"Mots clés" : Flamme_S - Cable fires	Nbre de pages : 37 Nbre de figures : 47
RESUME : Ce document présente les résultats de simulations numériques réalisées avec le code Flamme_S pour les scénarios de feu de chemin de câbles (voie de relais devant entrer en service en cas de dysfonctionnement de la voie principale). Ce travail a été réalisé dans le cadre d'un projet international visant à évaluer les modèles incendie appliqués à des feux dans des installations nucléaires.		
ABSTRACT : This report presents the results of numerical simulations achieved with the Flamme_S code on cable tray fires of redundant safety trains. This work has been done in the frame of an international collaborative project to evaluate fire models for nuclear power plant applications.		
Repère bureautique :00-930		

CEA CADARACHE · 13108 ST PAUL LEZ DURANCE CEDEX

Bt 346-IPSN/DRS/SESHP/GMEF - 4 : 04 42 25 31 77 - Fax : 04 42 25 48 74

TABLE OF CONTENTS

1. INTRODUCTION	6
2. DEFINITION OF THE PROBLEM	6
2.1 ROOM SIZE AND GEOMETRY	6
2.2 WALL, FLOOR AND CEILING	7
2.3 CABLES	7
3. PART I	7
3.1 MAIN PURPOSE AND SCENARIO	7
3.2 MODELLING OF THE PROBLEM WITH THE FLAMME_S CODE	8
3.2.1 <i>The trash bag fire</i>	8
3.2.2 <i>The cable</i>	9
3.3 NUMERICAL RESULTS	9
3.3.1 <i>Enclosed room</i>	9
3.3.2 <i>Ventilated room</i>	12
3.3.3 <i>Complementary study</i>	14
3.4 CONCLUSION OF THE FIRST PART	16
4. PART II	17
4.1 MAIN PURPOSE AND SCENARIO	17
1.2 MODELLING OF THE PROBLEM WITH THE FLAMME_S CODE	19
1.2.1 <i>The burning cable tray stack</i>	19
1.2.2 <i>The cable target (tray B)</i>	19
1.3 NUMERICAL RESULTS	20
1.3.1 <i>Enclosed room</i>	20
1.1.2 <i>Ventilated room</i>	24
1.4 CONCLUSION OF THE SECOND PART	29
5. CONCLUSION	29
6. REFERENCE	31
7. APPENDIX	32
7.1 APPENDIX 1	32
7.1.1 <i>Case 4 Door open</i>	32
7.1.2 <i>Case 5 Ventilation system on</i>	34
7.2 APPENDIX 2	35
7.2.1 <i>Enclosed cases (1,2,3,4,5,6,7,8,13)</i>	35
7.2.2 <i>Case 9</i>	37
7.2.3 <i>Case 10</i>	38

1. INTRODUCTION.

This report presents the results of the numerical simulations achieved with the two-zone model code Flamme_S on cable tray fires of redundant safety trains. This work has been done in the frame of an international collaborative project to evaluate fire models for nuclear power plant applications.

2. DEFINITION OF THE PROBLEM.

2.1 Room size and geometry.

A representative PWR emergency switchgear room has been selected for the benchmark exercise [1]. The room is 15.2 m deep, 9.1 m wide and 4.6 m high (see Figure 1). The room contains the power and instrumentation cables (trays A, C1, C2) for the pumps and valves associated with redundant safe-shutdown equipment (tray B). Both cable trays run the entire depth of the room, and are arranged in separate divisions and separated horizontally by a distance d.

The room has a door 2.4 m x 2.4 m located at the midpoint of the front wall and assumed to lead to the outside. The room also has a mechanical ventilation system with a flowrate of 5 volume changes per hour in and out of the room. The flowrate is assumed to be constant in the mechanical ventilation system. The midpoint of the vertical vents for the supply and exhaust air are located at an elevation of 2.4 m and have area of 0.5 m² each. The vents are supposed to be square and connect the room to the outside.

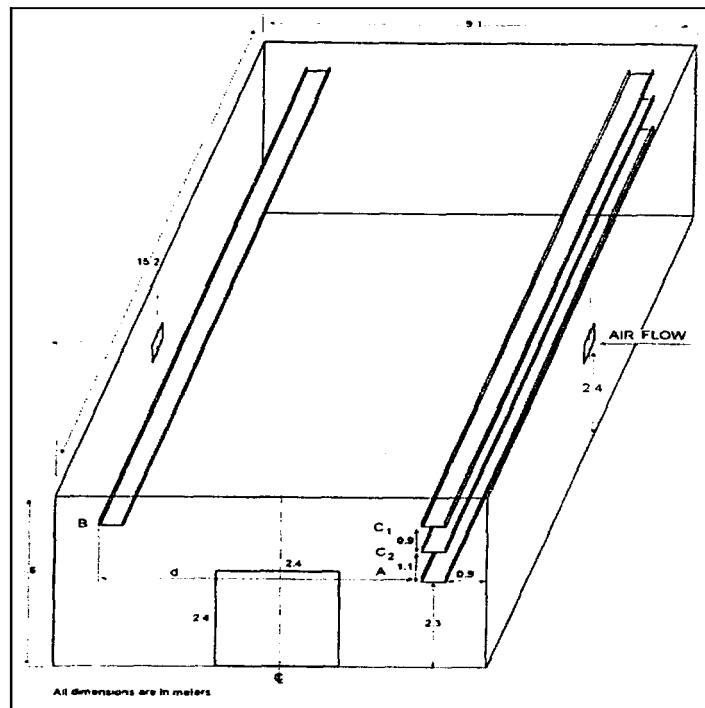


Figure 1: Geometry.

2.2 Wall, floor and ceiling.

The walls, floor and ceiling are 15.2 cm thick. The thermophysical data used in the numerical simulations are:

Specific heat	1000 J/kg.K
Thermal conductivity	1.75 W/m.K
Density	2200 kg/m ³
Emissivity	0.94

2.3 Cables.

The cable trays are 0.6 m wide and 0.08 m deep. As can be seen on the Figure 1, a horizontal distance d separates tray B from tray A. The thermophysical data used for cables are :

Heat of Combustion	16MJ/kg
Fraction of flame heat released as radiation	0.48
Specific heat	1040 J/kg.K
Thermal conductivity	0.092 W/m.K
Density	1710 kg/m ³
Emissivity	0.8

3. PART I.

3.1 Main purpose and scenario.

The objective of the Part I is to determine the maximum horizontal distance between a specified transient fire and the tray A that results in the ignition of the tray A (643 K). In this part, the transient fire is assumed to be a trash bag fire whose heat release rate is represented on the Figure 2:

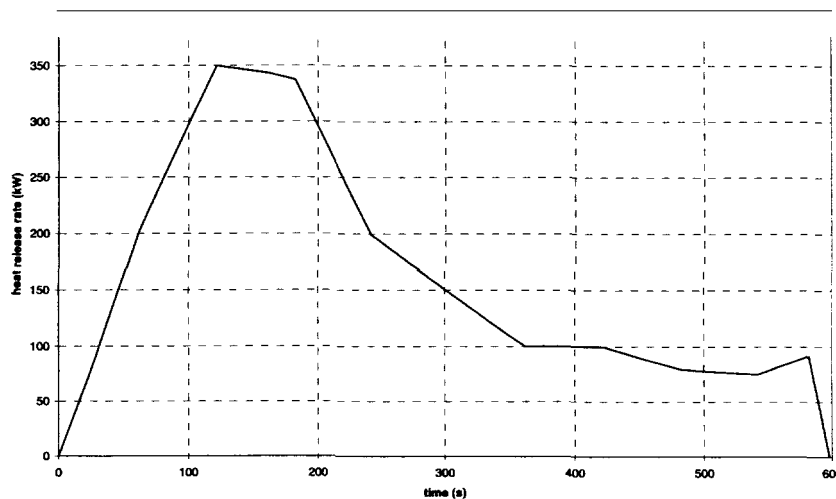


Figure 2: Trash bag fire - Heat release rate.

The trash bag is approximated by a cylinder with a diameter of 0.49 m and a height of 0.62 m. The mass of fuel is 4.06 kg and its heat of combustion is 24.1 MJ/kg with a fraction of 0.3 released as radiation.

The trash bag and the target (representing tray A) are located at the centre of the cable tray length. The target is assumed to be a single power cable with a diameter 50 mm at the bottom left corner of the cable tray A (see Figure 3).

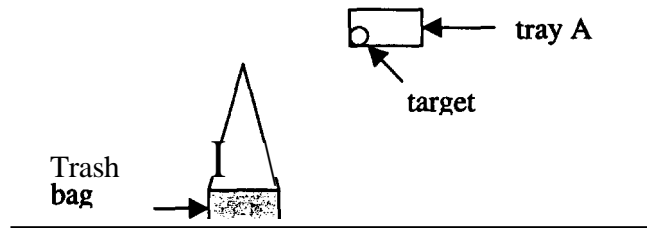


Figure 3: Part I - Trash bag fire.

In this first part, the following calculations are achieved:

- 1/ The horizontal distance between the midpoints of the trash bag and the tray A is successively 0.3 m, 0.9 m, 1.5 m and 2.2 m. In these simulations the ventilation system is off and the door is closed.
- 2/ The horizontal distance between the trash bag and the tray A is 2.2 m and the door is open.
- 3/ The horizontal distance between the trash bag and the tray A is 2.2 m and the ventilation system is on.

All the simulations of the Part I are summed up in the following table:

	Distance from fire (m)	Door	Ventilation system
Base case	2.2	Closed ¹	off
Case 1	0.3 ²		
case2	0.9		
Case 3	1.5		
Case 4		open	
Case 5			on

3.2 Modelling of the problem with the Flamme_S code.

3.2.1 The trash bag fire.

The fuel is assumed to be a trash bag containing wood (fir). The thermophysical data for wood are issued from the fuel data library available with the Flamme_S code. The data concerning the heat of combustion and the fraction of heat released as radiation have been

¹ For simulation with the door closed, a crack (2.4m x 0.005 m) at the bottom of the doorway is assumed

² A value in a cell indicates the parameter is varied from the base case

changed and are equal to the data advised in the definition of the benchmark exercise (24.1 MJ/kg for the heat of combustion³, 0.3 for the fraction of heat released as radiation).

The flame and the plume above the trash bag are described with the Heskestad model [2].

3.2.2 The cable.

In the Flamme_S code, a target such as a cable is represented by a rectangular slab. This slab can be divided in several meshes in the three directions. Hence, a complete description of the temperature field in the cable is available. In the modelling of a slab, the heat exchanges between the slab and its surroundings are only possible with the upper **and** lower faces of the slab⁴ (see Figure 4). That is why, the dimensions of the slab (width and depth) must be estimated in order (a minima) to:

- 1) have the same mass between the true cable and the slab,
- 2) have the same surface for heat exchanges.

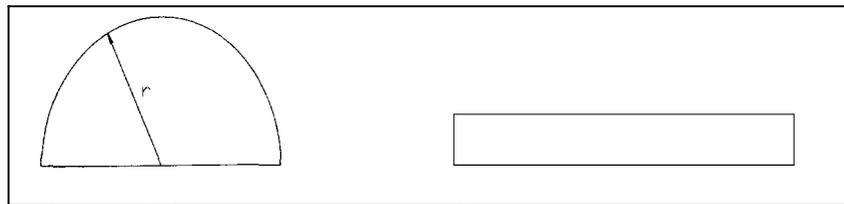


Figure 4: Modelling of the target with a rectangular slab.

Those two conditions impose the following dimensions for the slab:

$$a = \text{width} = \pi \cdot r \quad e = \text{depth} = r$$

In all the simulations of the **Part I**, the slab is divided in 1 (width) x 30 (depth) x 29 (length) meshes. With this cutting, the first mesh at the centre of the slab is 0.42 mm deep⁵.

3.3 Numerical results.

3.3.1 Enclosed room.

The first part of this study is devoted to the numerical simulations in the cases with no mechanical nor natural ventilation. We are interested here in the results of the calculations of the base case and cases 1, 2, 3.

³ The actual value of the heat of combustion of the wood is equal to 19.6 MJ/kg.

⁴ This comes from the fact that the "object" used to model the slab was initially devoted to the modelling of the wall, floor **and** ceiling.

⁵ More meshes in the "deep direction" induce high restriction in the time step (**CFL** like condition).

Heat release rate.

The Figure 5 shows the evolution of the heat release rate of the fire. Given the high volume of the room and the relatively low heat release rate of the fire, the oxygen molar fraction is always enough high to ensure the combustion until $t=590s$. At this time, the fire self extinguished for lack of fuel.

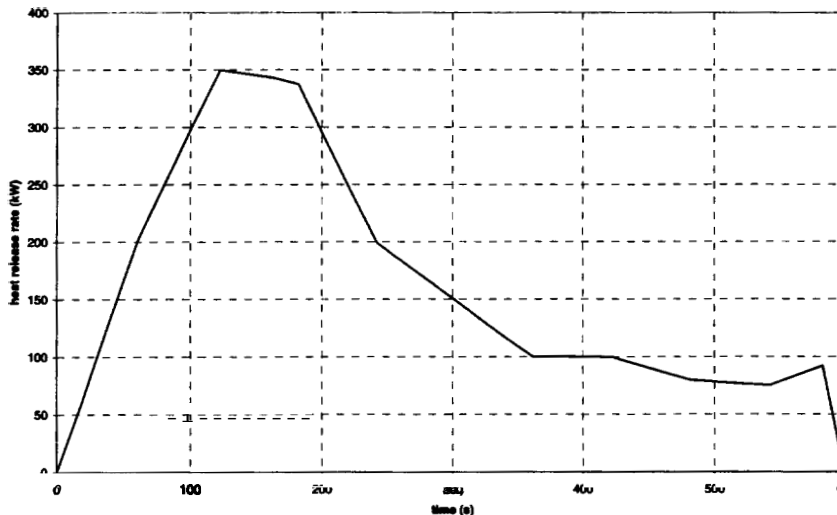


Figure 5: Heat release rate of the fire.

Temperature.

The analysis of the numerical results shows that the temperatures in the room are the same in all the enclosed room simulations. This observation shows that the localisation of the cable has a negligible effect on the whole thermal behaviour of the room. The Figure 6 shows the evolution of the room temperature. As shown in this figure, the high volume of the room associated with a relatively low heat release rate of the fire ($<350\text{ kW}$) induce low maximum temperatures in the room ($T_{max} < 80^{\circ}\text{C}$). This observation means that any failure or ignition of the target may be due either to radiant heat transfer from the flame or from convective heat transfer with the plume, but not from convective heat transfer with the hot gas layer.

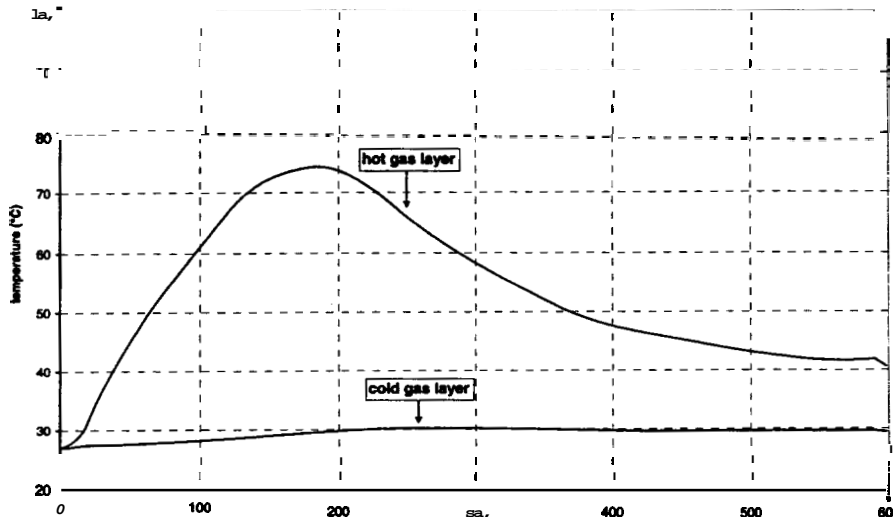


Figure 6: Room temperature.

The Figure 7 shows the evolution of the hot and cold layer depth. As can be seen on this figure, the target is in the hot gas layer from $t=160s$.

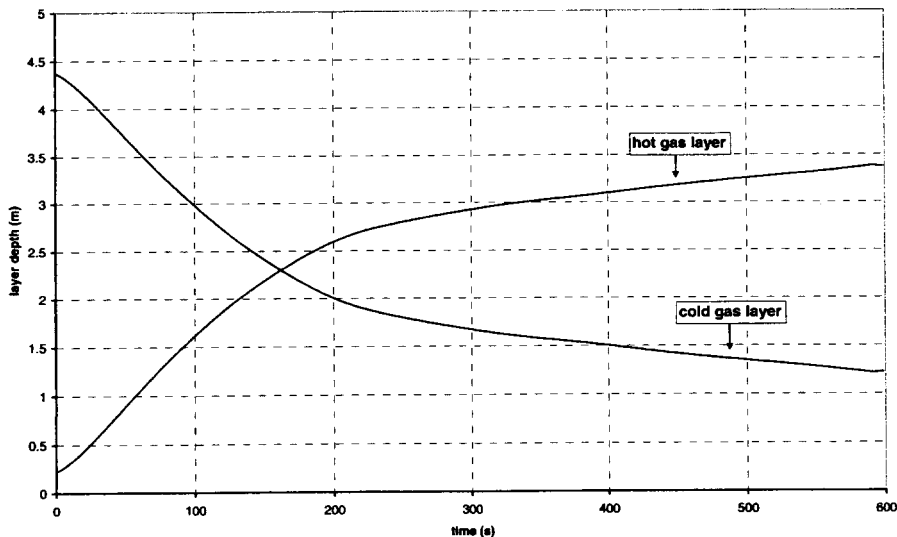


Figure 7: Gas layer depths.

The target.

As mentioned before, the heating of the cable is principally due to the radiant heat released by the flame and, given its position, to the convective heat transfer with the hot gas of the plume. The Figure 8 shows the temperature of the first mesh at the centre of the target. In the following of the text it will be referred as the maximum surface temperature of the target. The evolution of the temperature surface of the cable follows the heat release rate of the fire and starts decreasing when $t \approx 150s$. As can be seen on the Figure 8 and on the Figure 9 the ignition temperature is reached when the distance between the midpoints of the trash bag and tray is between 0.4m and 0.5m.

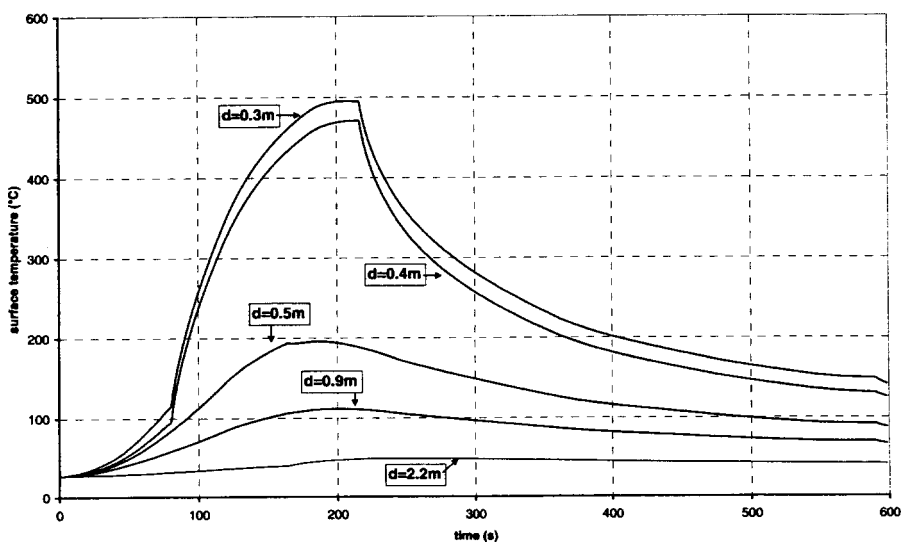


Figure 8: Temperature "surface" of the cable.

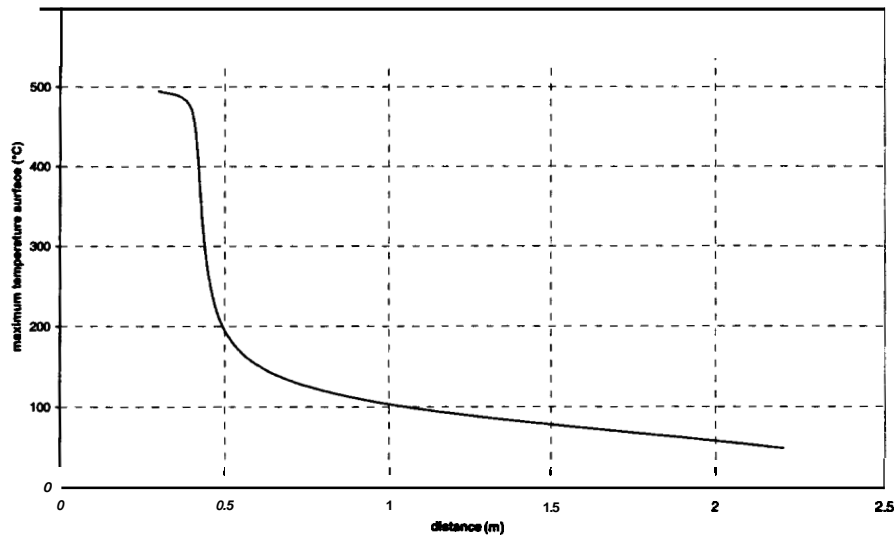


Figure 9: Maximum temperature "surface" of the cable.

The strong difference between the results with $d=0,4$ m and $d=0,5$ m comes from the fact that in the last case the cable is never in the plume of the fire (according to the calculations). The increase in the temperature for $d>0,5$ m is only due to the radiant heat released by the flame.

The Figure 10 shows the temperature of the central mesh. The low thermal conductivity of PVC induces a strong temperature gradient between the surface and the centre of the cable.

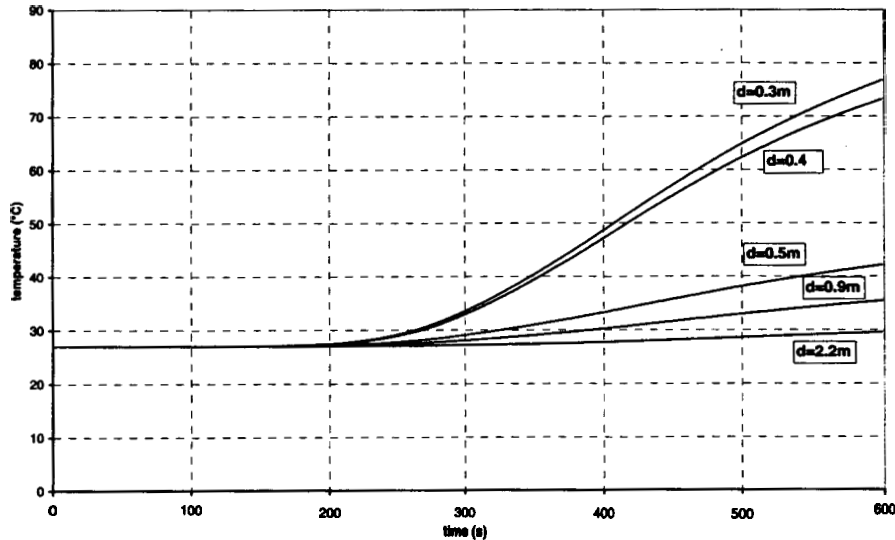


Figure 10: Temperature inside the cable.

3.3.2 Ventilatedroom.

The results obtained in ventilated configurations and with $d=2,2$ m are nearly the same as in the base case. As can be seen on Figure 11, the temperature in the room does not exceed 80°C . The results of both calculations are very near until $t=160$ s ; before this time the interface height is above the vents and the door and the mass flows due to ventilation only concern the lower layer.

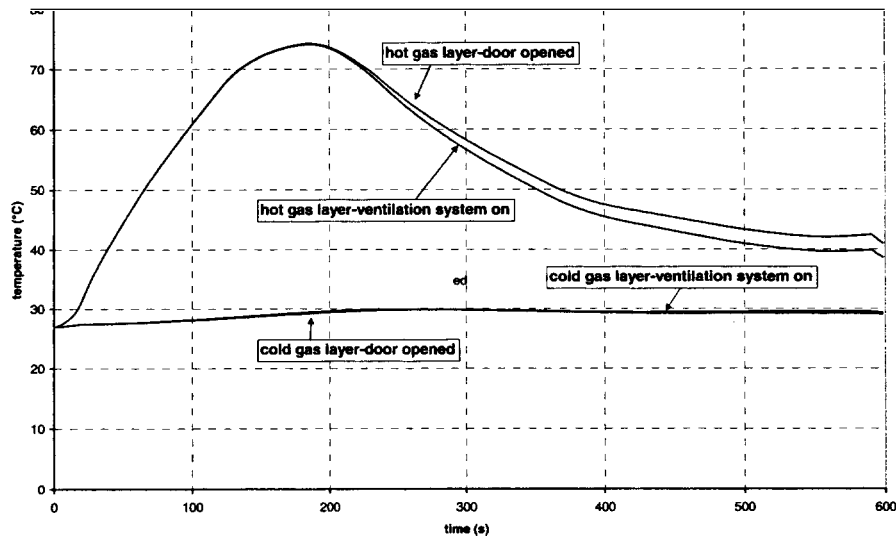


Figure 11: Temperature profiles for the cases with the door open and ventilation system on

The Figure 12 shows the cable temperature. The maximum temperature surface of the target is less than 60°C in both cases far from the ignition temperature. The break in the slope at $t \approx 160$ s corresponds to the time when the cable enters the hot gas layer (cf. Figure 35). From this moment, convective heat transfer with the gas of the room quickly increases since upper layer's gas are hotter than lower layer's ones.

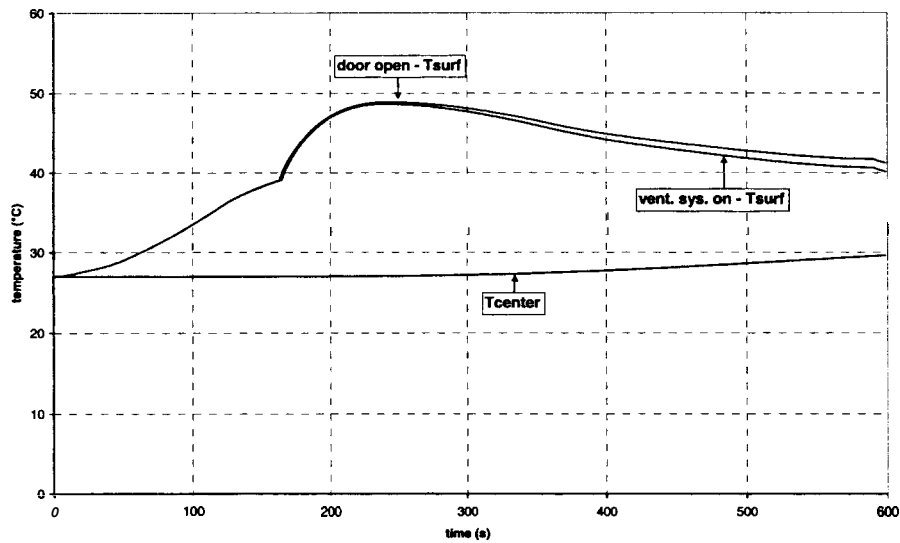


Figure 12: Cable temperature.

All the other results concerning the case 4 and the case 5 are reported in the Appendix 2.

3.3.3 Complementary study.

The calculation of the radiant heat transfer between the flame and the target is based on a classical point source approach. If r is the distance between the point source and the cable, the radiation heat on the cable is expressed as:

$$\Phi_{\text{target}} = \Phi_{\text{flame-rad}} \cdot \frac{\Omega}{4\pi} = \Phi_{\text{flame-rad}} \cdot \int \frac{dS}{4\pi r^2} \text{ (in W)}$$

where Ω is the solid angle, Φ_{target} is the radiant heat on the target, $\Phi_{\text{flame-rad}}$ the radiant heat released by the flame and dS the surface of the target "seen" by the point source.

When the target is cylindrical, dS remains constant and the solid angle decreases as the distance between the fire and the cable. The radiation heat on the cable only depends on r . On the other hand, when the cable is modelled as a slab (see Figure 13), the solid angle decreases as r increases and because of the decrease of dS . The radiation heat on the cable no more depends directly on r^6 .

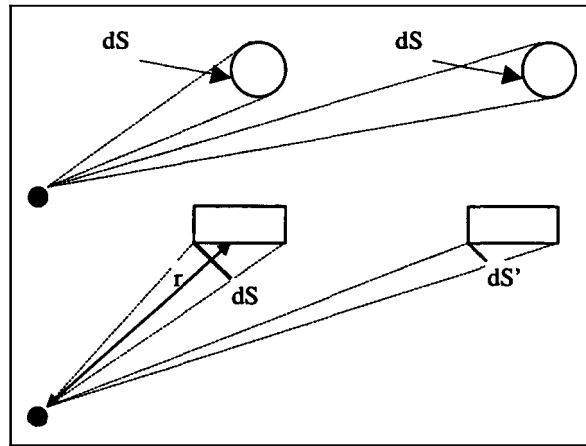


Figure 13: Radiant heat released on the target

In order to avoid this phenomenon, the problem has also been modelled in the following way: the target is located upon the fire source, the distance between the top of the fuel and the target being the same as in the real geometry.

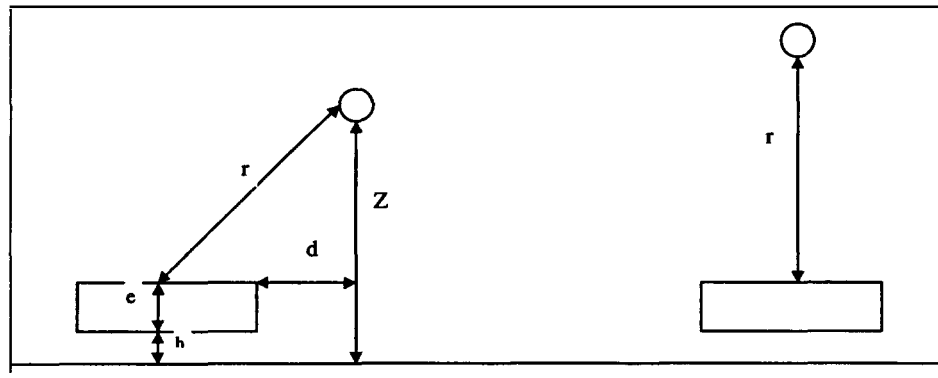


Figure 14: Real geometry (left) and modelled problem (right).

⁶ Remember that in our modelling, only two opposite faces are involved in heat transfer.

The distance between the fuel surface and the target is given by :

$$r^2=(R+d)^2+(Z-h-e)^2$$

Where: R = the radius of the fuel surface,
 e = the depth of the fuel (=0.048m),
 h = the height of the fuel (=0.62m).

If H is the absolute height of the target in the modelled problem, the relation between d and H is:

d (m)	0.15	0.3	0.9	1.5	2.2
H (m)	2.36	2.40	2.69	3.09	3.65

Comments:

1/ In this approach convective heat exchange between the hot gas layer and the cable depends on the distance between the fire source and the target. The consequences of this difference are probably low since, as can be seen in the previous parts, the decrease of the interface height is quite fast and the increase of the temperature of the hot gas layer is relatively small.

2/ The source of the code has been modified in order that the convective heat exchanges on the target, which is now in the fire plume, are not calculated with the plume temperature.

The Figure 15 shows the maximum temperature surface of the cable when heated by radiant heat from the flame.

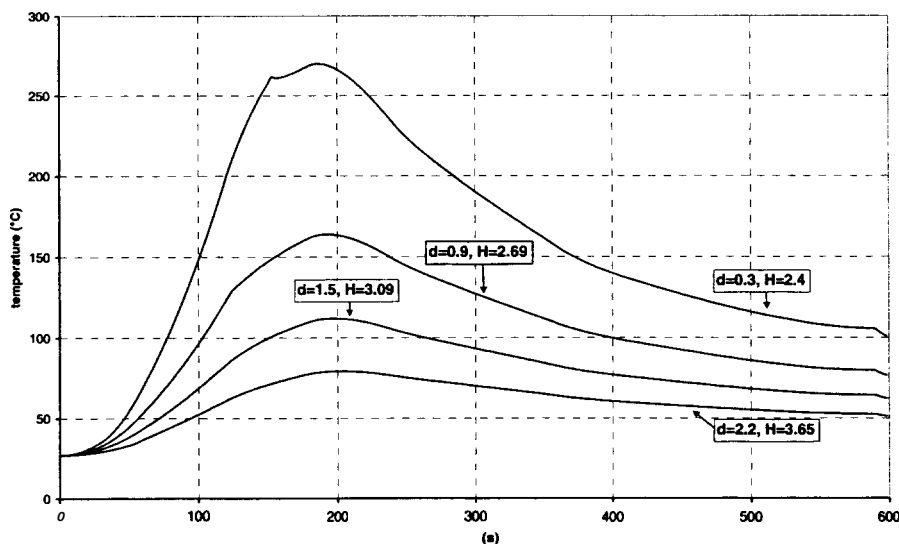


Figure 15: Temperature "surface" at the centre of the target.

Several comments can be made:

1/ The maximum temperature surface never reaches the ignition temperature (370°C).

2/ The maximum temperature surface decreases when the distance between the fire and the target increases.

3/ The sudden slopes changes in the temperature profiles correspond to the time when the target enters the hot gas layer (ex: $d=0.3$ m, $t=150$ s). At this time, a part of the radiant heat released by the flame is absorbed by the gas.

4/ For $t > 200$ s the maximum surface temperature decreases. This corresponds to the fact that the heat release rate of the fire decreases and that the gas of the hot gas layer is colder than the target.

The Figure 16 shows the radiant heat flux on the mesh at the centre of the target. The strong decreases observed at $t=150$ s for $d=0.3$ m and at $t=120$ s for $d=0.9$ m correspond to the time when the target enters the hot gas layer (see also Figure 7).

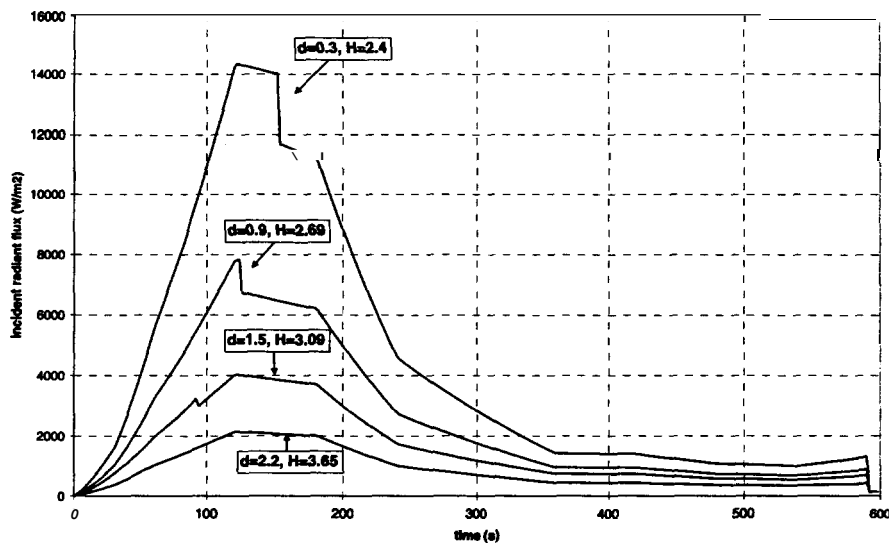


Figure 16: Incident radiant heat flux on the target.

It is also interesting to highlight that the maximum heat flux calculated for $d=0.3$ m is only slightly higher than 14 kW/m^2 and that the target receives this flux only during a short time. This radiant heat flux is equal to the critical heat flux found in the literature for the PVC [4]. Maybe this explains the reason why the ignition temperature is never reached in this study.

3.4 Conclusion of the first part

The numerical simulations of the first part show that, given the dimensions of the geometry and the relatively low heat release rate of the fire, the ignition or damage of the cable is unlikely except when it is located in the fire plume.

4. PARTII.

4.1 Main purpose and scenario.

The objective of the part II is to determine the damage time (t_d) of the cable tray **B** for several heat release rates of the cable tray stack fires (trays A, C1 and C2) and horizontal distance, d (see Figure 1). The effect of target elevation and ventilation will also be examined.

In this part the fire is supposed to be a burning cable tray stack. As the modelling and the prediction of the heat release rate of such a fire are extremely difficult (pyrolysis, flame propagation, ...), the heat release rate is considered as an input of the problem. The peak heat release rate (Q_0) for the whole cable tray stack is between 1-3 MW. The ignition period is modelled as a t -squared growth:

$$Q(t) = Q_0 (t/t_0)^2 \quad \text{where } t_0 = 10 \text{ min}$$

The fire duration (Δt) is 60 min at peak heat release rate and then the decay period is described in the same way as the ignition growth:

$$Q(t) = Q_0 \left[\left(1 - \frac{x_e}{x_e - 1}\right) \left(\frac{t}{t_0 + \Delta t}\right)^2 + \frac{x_e}{x_e - 1} \left(\frac{t}{t_0 + \Delta t}\right) \right]$$

where
$$x_e = \frac{(2t_0 + \Delta t)}{t_0 + \Delta t}$$

The theoretical heat release rate for the burning cable tray stack used in this part is displayed on the Figure 17.

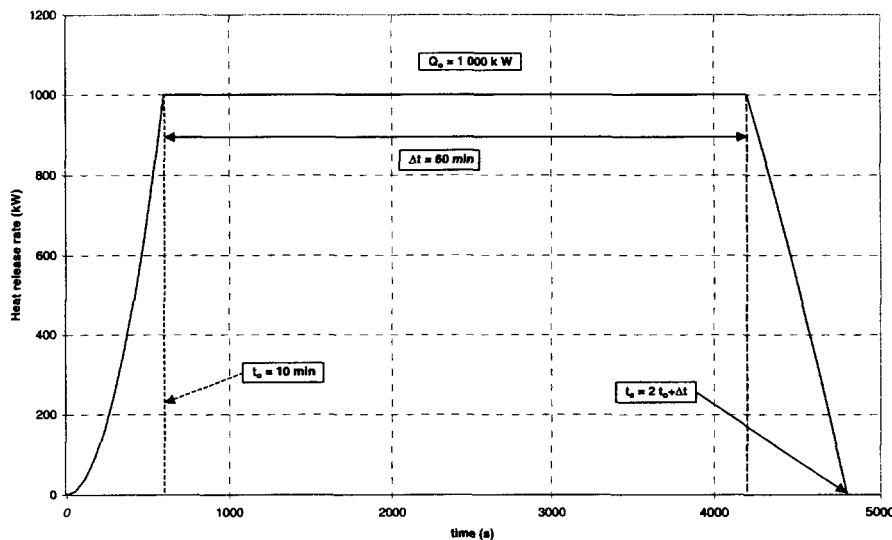


Figure 17 : Burning cable tray stack - theoretical heat release rate

The ignition and burning of the cable tray stack is modelled as one fire. The heat source (trays A, C1 and C2) is at the centre of the cable tray length and width and at the elevation of the

bottom tray **C2 (3.4 m)**. The fire source is assumed to be the entire length of tray **C2 (15.2 m)**, width **(0.6 m)** and height **(0.24 m)**. In **this** part, the target is a single power cable (like in part I) or **an** instrumentation cable made of **PVC** with a diameter of **50 mm** or **15 mm** respectively. The cable is assumed to be damaged when its core reaches **200°C**. The target is located at the bottom right corner of cable tray B (see Figure 18).

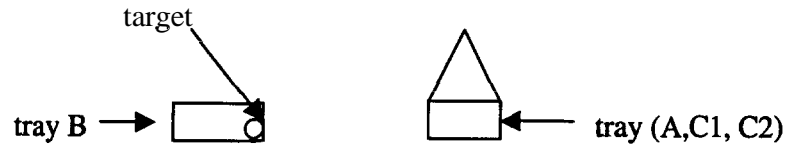


Figure 18 :Part II – Burning cable tray stack (A, C1, C2)

In this section, the following calculations are performed:

1/ The peak heat release rate for the cable tray stack is equal to **1 MW**; the horizontal distance (d) between the fire and the target is successively **3.1 m, 4.6 m** and **6.1 m**.

2/ The peak heat release rate varies from **2 to 3 MW** at a horizontal distance $d = 3.1 \text{ m}, 4.6 \text{ m}, 6.1 \text{ m}$.

3/ The door is closed and the ventilation system initially runs; the door is open and the ventilation system shuts after **15 min**.

4/ The door is open and the ventilation system is on throughout the simulation.

5/ The tray B is **2.0 m** above tray A or at the same elevation as the tray A.

6/ The target is an instrumentation cable with a diameter of **15 mm**.

All the cases considered in this part are summarised in the table thereafter:

	HRR (MW)	d (m)	Door	Vent Sys.	Target	Elev ⁷ . (m)
Base case	1	6.1	Closed⁸	Off	Power	1.1
Case 1		3.1⁹				
Case 2		4.6				
Case 3	2	3.1				
Case 4	2	4.6				
Case 5	2	6.1				
Case 6	3	3.1				

⁷ Height above tray A

⁸ For simulations with the door closed, a crack (2.4m x 0.005 m) at the bottom of the doorway is assumed

⁹ A value in the cell indicates the parameter is varied from the base case

SESHP/GME/IPS/FLS/C60/RP/00.930	Study of cable tray fires of redundant safety trains with the Flamme_S code.	
---------------------------------	--	--

Case 7	3	4.6				
Case 8	3	6.1				
Case 9			Open>15 min	Off>15 min		
Case 10			Open	On		
Case 11						2.0
Case 12						Same (0.)
Case 13					Instrument	

4.2 Modelling of the problem with the Flamme_S code.

4.2.1 The burning cable tray stack

The fuel is assumed to be a cable tray stack made of PVC. The thermophysical data for PVC are derived from the fuel data library available with the Flamme_S code except those provided by the definition of the benchmark (see § 2.3). The burning cable tray stack has been divided into ten smaller fire sources that are 1.52 m long, 0.6 m wide and 0.24 m high. This modelling of the fire source leads to a better description of the radiative exchanges between the flame and the target than with only one radiative source point set in the middle of cable tray A. Besides, the Flamme_S code prohibits the use of the Heskestad's correlations for the linear fire source (i.e length/width > 3). In the calculations, the given mass fractions for CO and soot have been used to deduce the others. The molar fractions of the combustion species introduced in the Flamme_S data files are listed in the following table :

Species	Molar fraction
CO ₂	0.9636
CO	0.1406
soot	.8958
H ₂ O	1.0
N ₂	5.8647
HCl	1.0

The lower oxygen limit in the calculations is set to 12%.

4.2.2 The cable target (tray B)

The target (tray B) has been represented by a vertical rectangular slab (see § 2.3). Its thickness and width depend upon its nature:

	Width (m)	Thickness (m)
Power cable	0.078	0.025
Instrumentation Cable	0.0236	0.0075

In all the calculations performed in the second part, the target has been divided in 30 (width) x 1 (depth) x 10 (length) meshes.

4.3 Numerical results.

4.3.1 Enclosed room.

The first part of the study deals with the simulations devoted to the enclosed room (base case, cases 1 to 8 and case 13). Remember that there is only a crack at the bottom of the doorway (2.4 m x 0.005 m).

Actual heat release rate

The evolution of the actual heat release rate as a function of time is shown in the Figure 19. The fire is quickly into the upper layer (see Figure 22). Given the volume of the room and the lower oxygen limit (12 %), the fire self-extinguishes due to the lack of oxygen in the upper layer (see Figure 20). As expected, the extinction delays decrease with the increase of the mass burning rate (i.e. with the peak heat release rate). The different extinction times are listed in the following table :

Q_o (MW)	Extinction delay (s)
1	720
2	556
3	484

After the fire extinction, the oxygen molar fraction in the upper layer remains constant because the interface height behaves as a fictitious solid surface¹⁰ (see Figure 20). In the cooler zone, the oxygen concentration remains constant to its initial value.

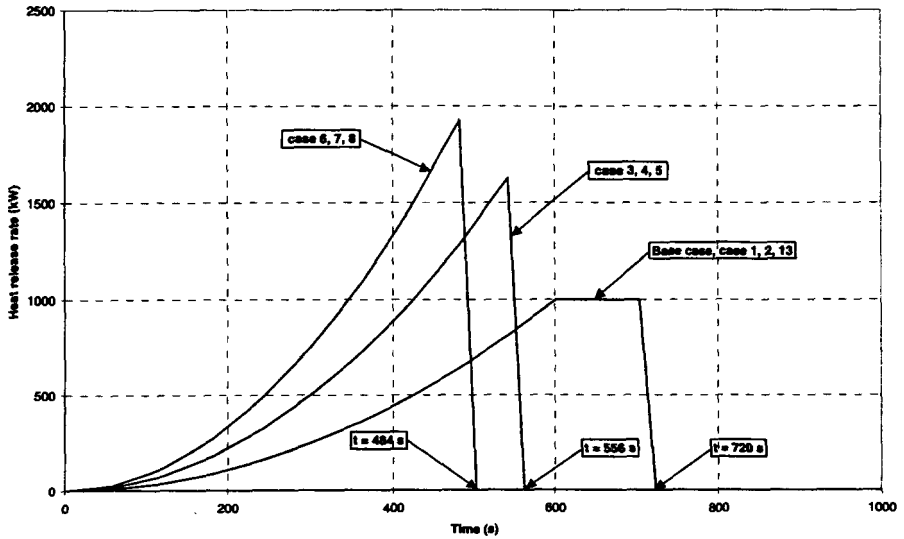


Figure 19 : Actual heat release rate

¹⁰No mass flow enter or leave the layers

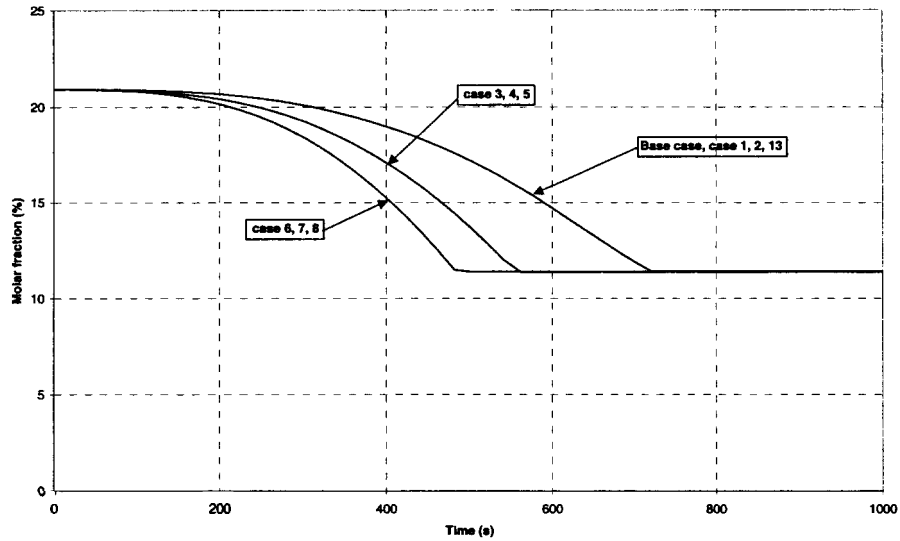


Figure 20 :Oxygen molar fraction in the upper layer

Upper and lower layer temperature

The analysis of the numerical results shows that the temperature profiles in the upper layer display the same tendency as the heat release rate (see Figure 21): the higher the peak heat release rate, the higher the maximum temperature in the upper layer. These temperatures are summed up in the following table :

Case	Maximum Upper layer temperature (°C)
Base case, Case 1, 2, 13	192
Case 3, 4, 5	244
Case 6,7 , 8	267

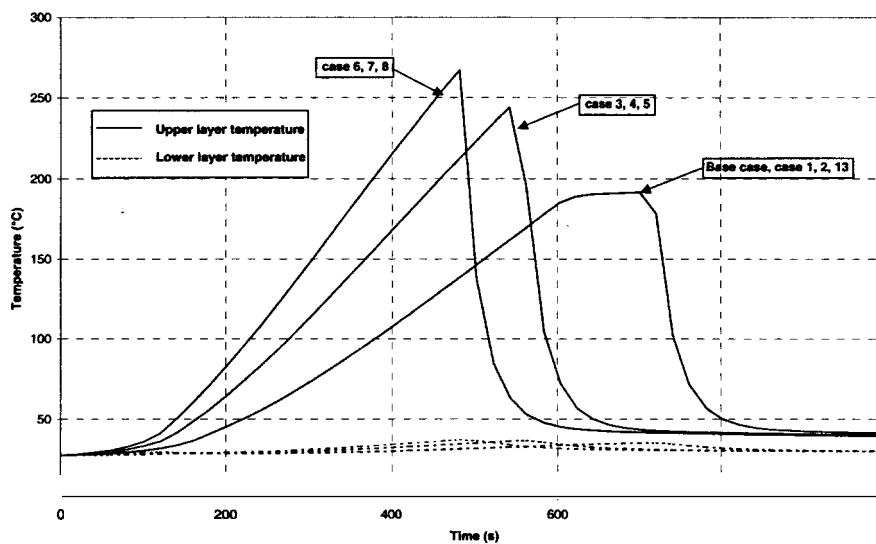


Figure 21 :Upper and lower layer temperatures

The Figure 22 also shows that the **shift** for the lower zone temperature is weak.

Gas layer depth

The Figure 22 displays the gas layer depth for all cases corresponding to the enclosed room. As shown in the figure, each curve has two inflexion **points**. The first one is reached when the interface height is near the upper surface of the burning cable tray stack. Beyond this moment, there isn't any more fresh air going into the upper layer from the cooler region throughout the plume. Nevertheless, due to the burning of the cable tray the combustion products go on filling out the upper layer. Therefore, the thickness of the lower layer decreases far below the fire place. When the fire self-extinguishes, the second inflexion point is reached. Beyond this moment, the quick cooling of the hot gases results in an increase of the interface height.

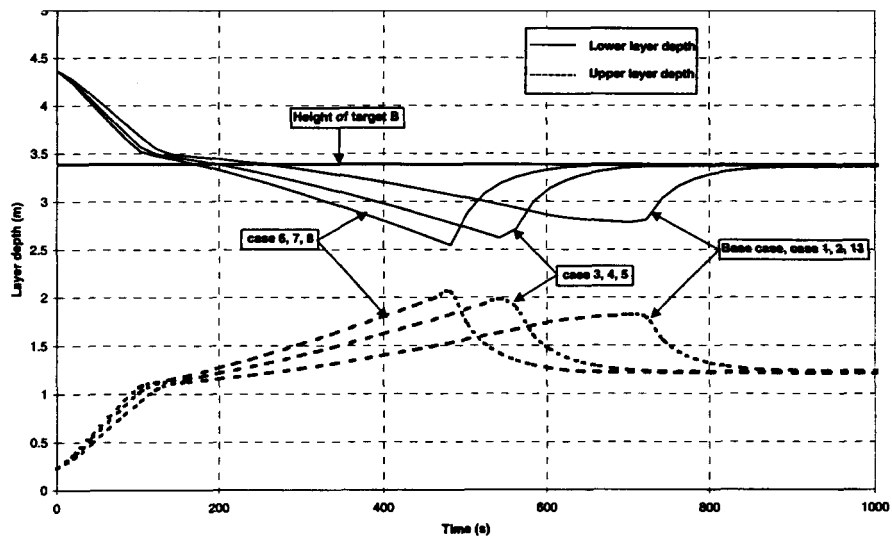


Figure 22 : Gas layer depth

The target

The temperature profiles at the surface and centerline of the target are displayed on the Figure 23. Each surface temperature profile displays a sudden change in its slope soon after the ignition of the cable. At this time, the target is plunged into the upper layer. The emissivity of the hot gases is around **0,5** and tends to increase. A non negligible amount of the fraction of heat released by the flame as radiation is absorbed by the hot gases. Thus, the increase of the target temperature is mainly due to the convective and radiative heat exchange between the target and the gases. Whatever the case, the **maximal** surface temperature of the target is always lower than the damage temperature (200°C) (see the following table) :

	Target maximal surface temperature (°C)
Base case, Case 1,2	130
Case 3, 4, 5	154
Case 6, 7, 8	161
Case 13	148

Besides, the core temperature of the target is also far below the surface temperature due to the value used for the thermal conductivity coefficient for PVC (0.092 W/mK) except for the case 13. In the case 13, the core temperature is much higher (see Figure 23) because the diameter of the instrument cable is indeed three times less than that of the power cable.

For the base case and the cases 1, 2, 13, the maximal upper layer temperature is even less than 200°C . Obviously, the target won't never be damaged. For the other cases, the comparison of the fire duration with the time needed for heat to reach the core of the target gives an insight of the reasons why the target will likely never be damaged. Remember that a rough estimate of how long it will take the back of the wall to feel an increase in the temperature on the front face is given by the following formula : $t_p \approx \frac{e^2}{16(\lambda/\rho c)}$ [3].

where e is the wall thickness, λ the thermal conductivity, ρ the density and c the specific heat.

	Thermal penetration time (s) (to reach the core of the cable)	Fire duration (s)
Power cable	200	720 (base case)

For the power cable, both characteristic times have the same magnitude. It consequently takes a non negligible amount of time to heat the whole cable (see Figure 23). For the instrument cable, with a short delay, the centerline temperature profile displays the same tendency as the surface temperature profile because the thermal penetration time is small in comparison with the fire duration.

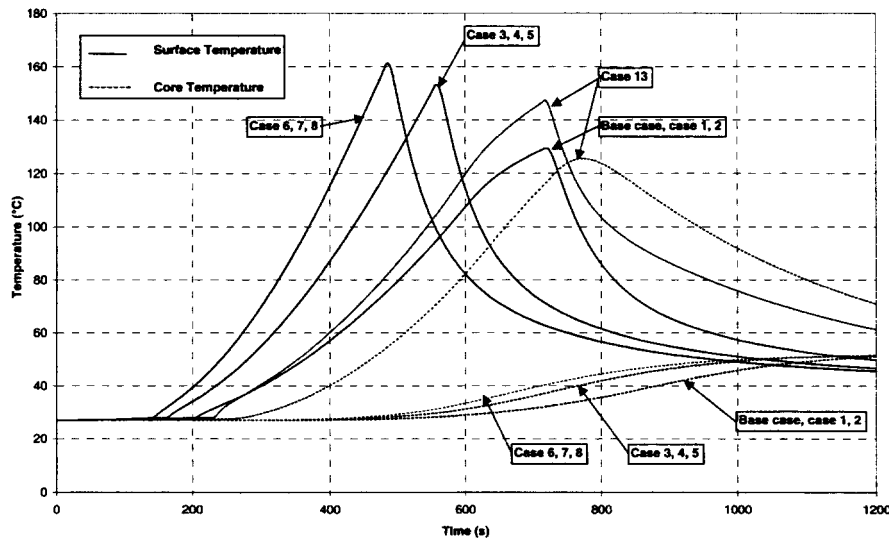


Figure 23 : Cable temperature profiles (target)

As the heat of the tray B mainly results from the thermal exchanges with the hot gases, the distance d between the target and the burning cable tray stack has no effect upon the temperature profiles in the target.

Additional results are given in the Appendix 2.

4.3.2 Ventilated room.

Case 9.

This case is different from the base case because of the ventilation conditions. The door is closed until 15 minutes at the time when the mechanical ventilation is stopped. The Figure 24 shows the evolution of the heat release rate of the cable fire. Despite the mechanical ventilation, the fire self-extinguishes at $t=720$ s for lack of oxygen.

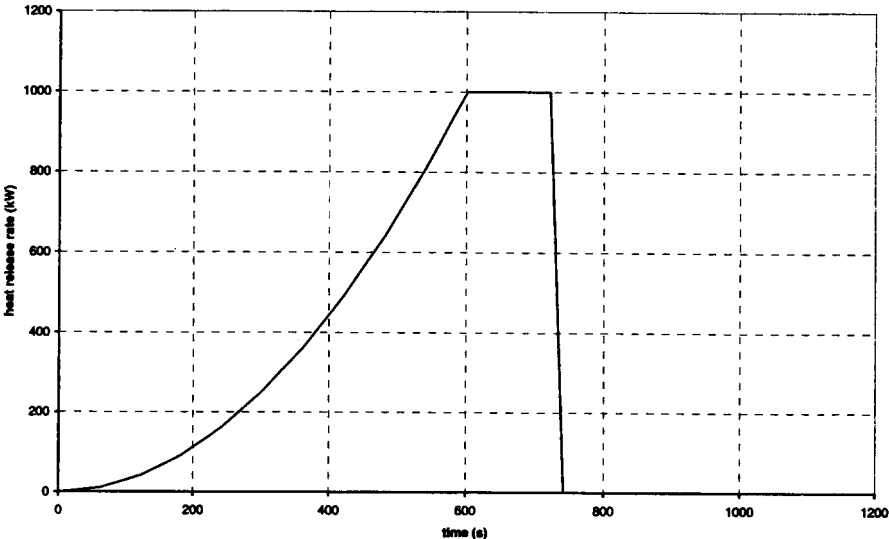


Figure 24: Heat release rate.

As can be seen on the Figure 25 the fire source is quickly ($t=200$ s) in the upper layer where the oxygen concentration reaches 12% at $t=720$ s (Figure 26). In this case the fire duration is **too** short for the ventilation effects to be felt.

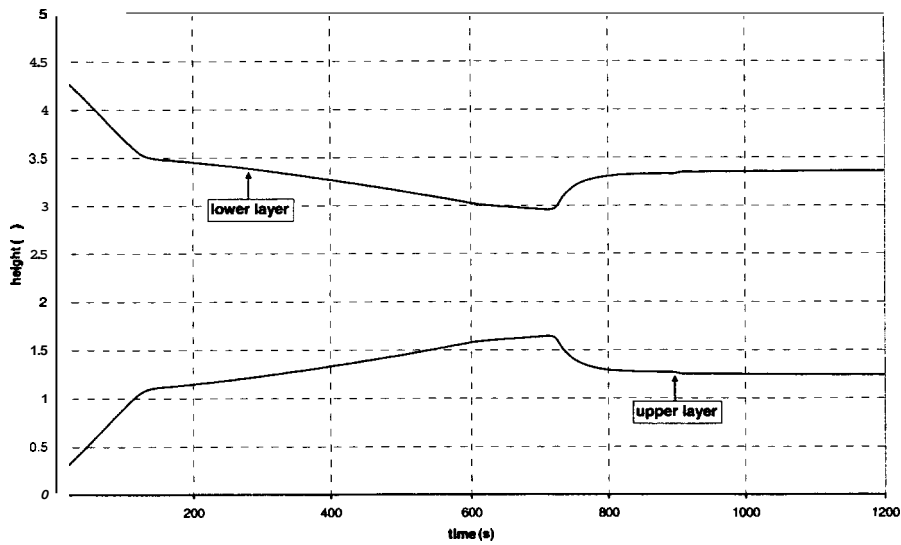


Figure 25: Depth of upper and lower layers.

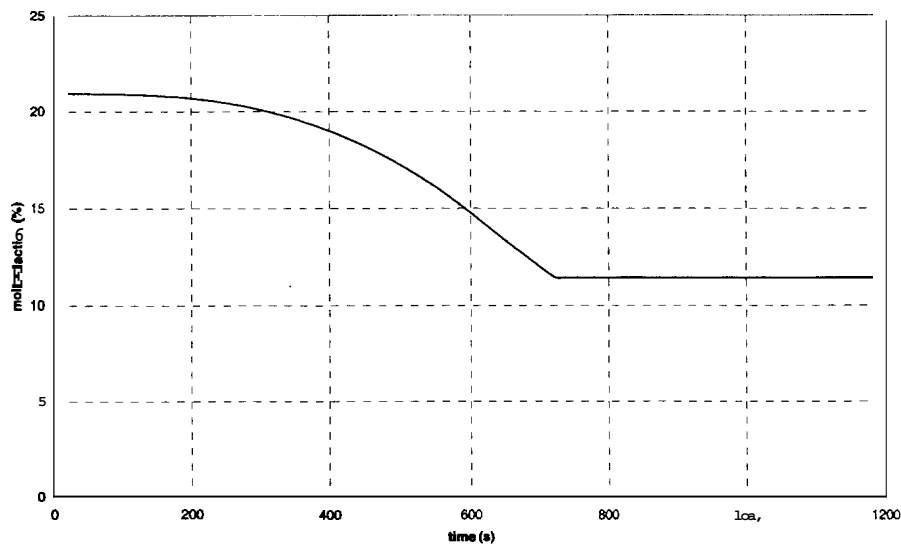


Figure 26: Oxygen molar fraction in the upper layer.

The temperature profiles in the room (Figure 27) show the same tendency as the heat release rate of the fire. The maximum temperature does not exceed 200°C and **this** explains the reason why the target remains far under the damage temperature (Figure 28).

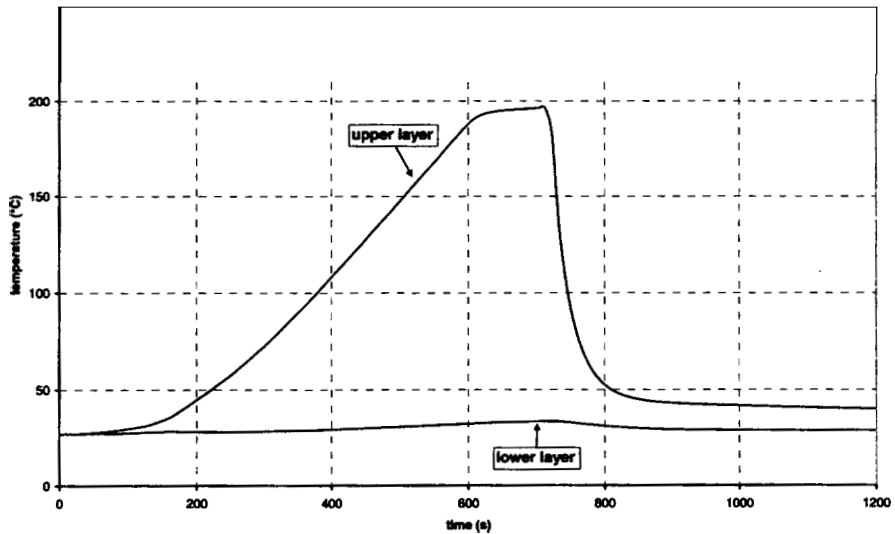


Figure 27: Room temperatures.

The sudden slopes change in the cable surface temperature at $t=200s$ corresponds to the time when the target enters the upper layer. At this time the convective heat exchange between the cable and the gas quickly increases because of the relatively high temperature of the gas of the upper layer.

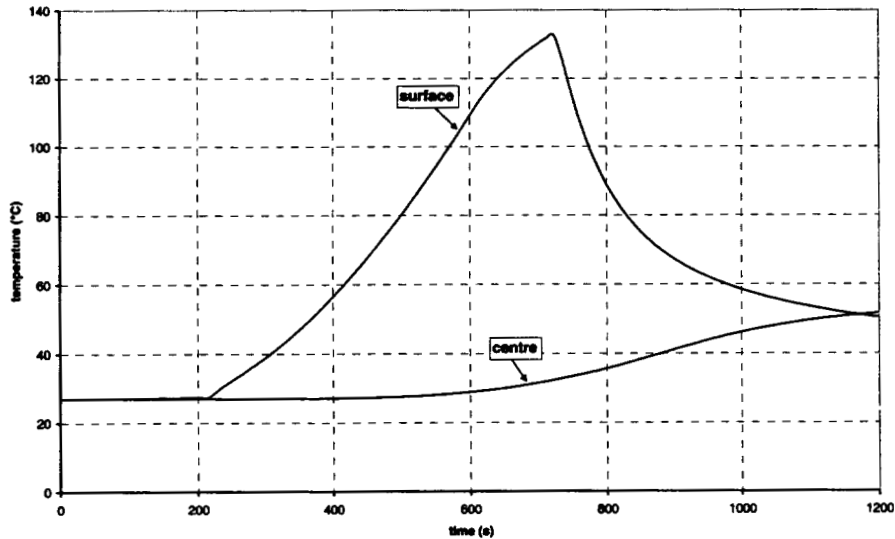


Figure 28: Cable temperature (target).

Complementary results are presented in the Appendix 2.

Case 10 and 10b.

In the case 10, the door is open and the ventilation system is on during all the fire duration. The case **10b** is a complementary simulation in which the elevation of the cable fire is 2.3 m (height of the cable tray **A**). This last simulation aims at studying the effect of the fire elevation in the model.

The Figure 29 shows the heat release rate of the fire in the cases 10 and 10b. In the first case, the fire self extinguishes at $t=720$ s for lack of oxygen whereas in the second case the fire reaches the end of the imposed HRR.

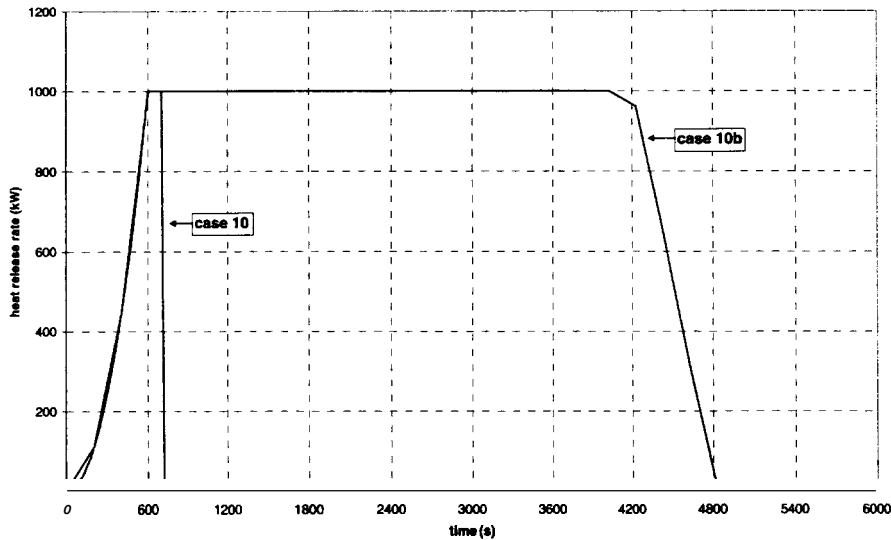


Figure 29: Heat release rate of the fire.

This difference is directly involved to the elevation of the fire source. In the case 10, the fire enters rapidly the upper layer of the room where the oxygen molar fraction reaches 12% at $t=720$ s. In the case 10b, the interface height reaches the bottom of the mechanical vents before the fire self-extinguishes for lack of oxygen (Figure 31). From this time, the upper layer is supplied with fresh air from the outside and the oxygen molar fraction remains enough to ensure the combustion (Figure 30).

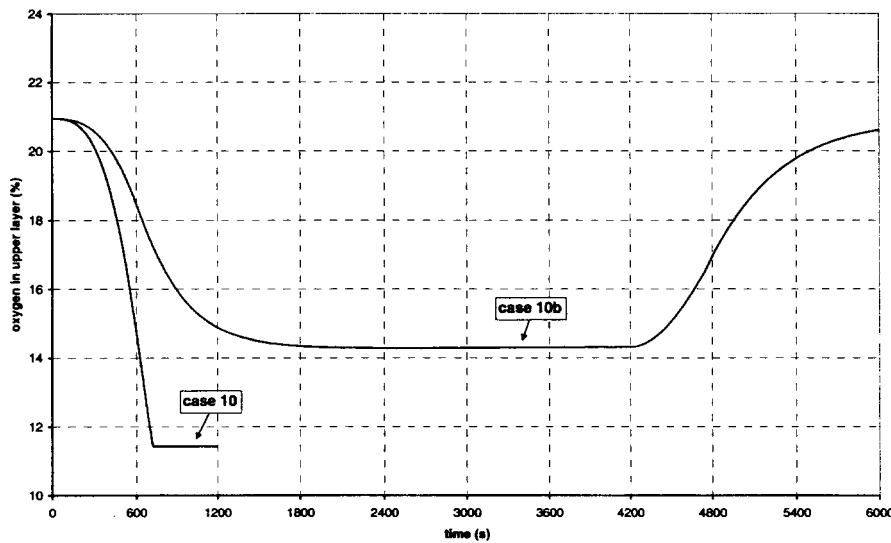


Figure 30: Oxygen molar fraction in the upper layer.

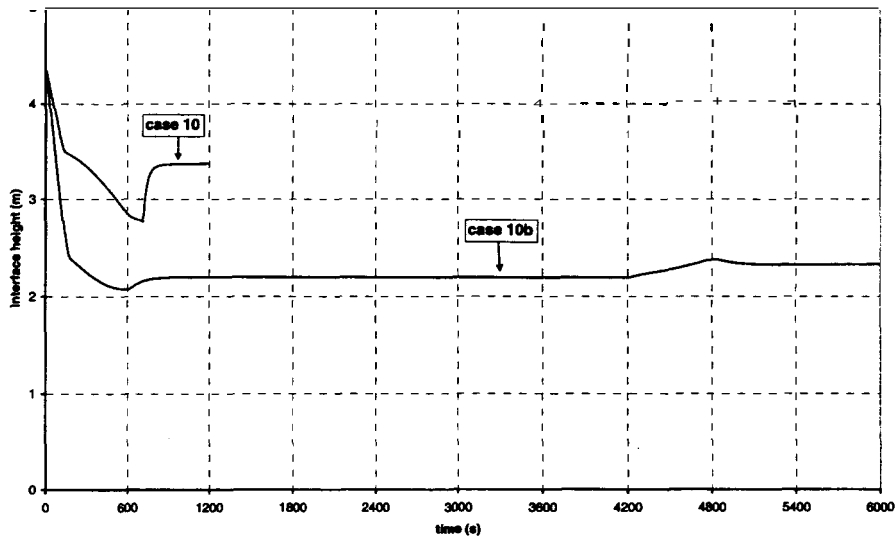


Figure 31: Interface height in the room.

The temperature profiles in the room show the same evolution as the heat release rate of the fire. The temperature increase in the room is quicker in the case 10 than in the case 10b at the onset of the fire. This comes from the fact that in the second case the dilution of the combustion products with the *air* entrained by the plume in the upper layer is more important. On the other hand, one can observe that in the case 10b the cable surface temperature exceeds 200°C at the end of the fire. In the case 10, the cable surface temperature does not reach 150°C because of the short duration of the fire.

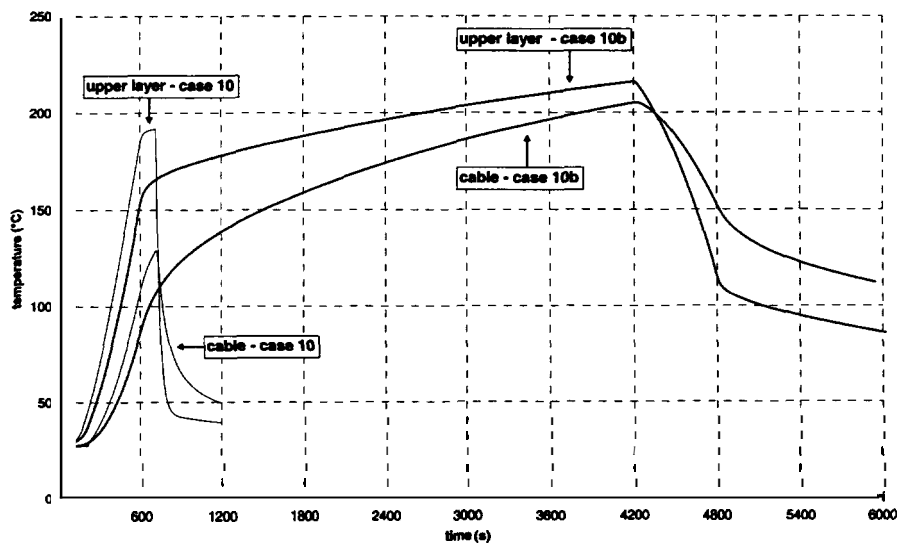


Figure 32: Cable surface and room temperature.

These simulations show the strong influence of the fire elevation in the current modelling of the problem.

Complementary results for the case 10 are reported in the appendix 2.

Cases 11.12

The difference between these cases and the base case is the elevation of the target which is 2 m (case 11) or 0 m (case 12) above the cable tray **A**. The elevation of the target has no effect on all the properties of both layers. Furthermore, for the same elevation as the cable tray **A**, the target is always in the cooler zone during all the simulation. Thus, the temperature of the whole target keeps nearly constant (around 30°C).

As the ceiling jet phenomenon is not modelled in the Flamme_S code, a rise in the elevation of the target (2 m above the tray **A**) leads to the same results as those obtained for the base case.

4.4 Conclusion of the second part

In the second part, the heating of the cable tray **B** is mainly due to the thermal exchanges with the hot gases. Whatever the case, the tray **B** is likely never damaged because the surface temperature of the target is below the damage temperature advised for the cable (200°C). For the enclosed room, the elevation of the target doesn't matter for the calculations because the ceiling jet effect is not taken into account.

From a calculation point of view, the elevation of the fire seems to be much more important. For example, when the fire is set to the elevation of cable tray **A** ($Q_0 = 1$ MW), the fire reaches the end of the imposed heat release rate leading to higher temperatures in the hot gases. In this case, near the end of the fire, the surface temperature of the target is slightly above the specified damage temperature. But even in **this** case, the target is not damaged.

5. CONCLUSION.

This report is devoted to a study of cable tray fires of redundant safety trains with a two-zone model. The aim of this work is to evaluate fire models for nuclear power plant applications. All the calculations have been performed with the 2.2 version of the FLAMME_S / SIMEVENT code.

The power and instrument cables trays (tray **A**) associated with the redundant safe shutdown equipment (tray **B**) are set in a representative PWR emergency switchgear room. They are arranged in separate divisions and separated horizontally by a distance d .

The study is divided in two parts. The purpose of the first one is to determine the maximum distance between a specified transient fire and the cable tray **A** which results in the ignition of the cable tray. The fire is assumed to be a trash bag containing wood. The aim of the second part is to evaluate the damage time of the redundant safe shutdown equipment (tray **B**) for several peak heat release rates of the cable tray stack **A** (1 - 3MW) and various horizontal distance d (3.1 m, 4.6 m, 6.1 m). In this part the cable trays are supposed to be made of PVC. The ignition of the cable fire is modelled of as a t-squared growth. The same modelling is used for the extinction of the fire.

The calculations achieved in the part **I** show that the heating of the cable tray **A** is mainly due to the fraction of energy released by the flame as radiation and, given the location of the trash in the room, to the convective exchanges with the plume. The main results of the numerical

SESHP/GME/IPS/FLS/C60/RP/00.930	Study of cable tray fires of redundant safety trains with the Flamme_S code.	
---------------------------------	--	--

simulations are that, given the size of the switchgear room and the relatively low heat release rate of the transient fire (**350 kW**), the ignition or damage of the cable tray **A** is unlikely except when it is in the plume of the fire.

In the second part, the analysis of the numerical results shows that the heating of the cable **tray B** principally results from the thermal exchanges with the hot gases of the upper layer. As in part I, the damage of the redundant cable **B** is unlikely. Furthermore, the elevation of the target in the room has no effect upon the results because in the Flamme_S code the ceilingjet phenomenon is not modelled.

6. REFERENCE.

1. MONIDEEP DEY

“Benchmark exercise #1 - Cable tray fire of redundant safety trains.”

International Collaborative Project to Evaluate Fire Models for Nuclear Power Plant Application - Revised september 11 - 2000.

2. HESKESTAD G.

“Fire Plumes”

The SFPE Handbook of Fire protection Engineering -1995.

3. QUINTIERE J. G.

“Heat Transfert”

Principles of Fire Behavior - 1998

4. TEWARSON A.

“Generation of heat and chemical compounds in fire.”

The SFPE Handbook of Fire Protection Engineering - 1995.

7. APPENDIX.

7.1 Appendix 1.

This appendix presents the results of the door open and ventilation system on cases.

7.1.1 Case 4- Door open.

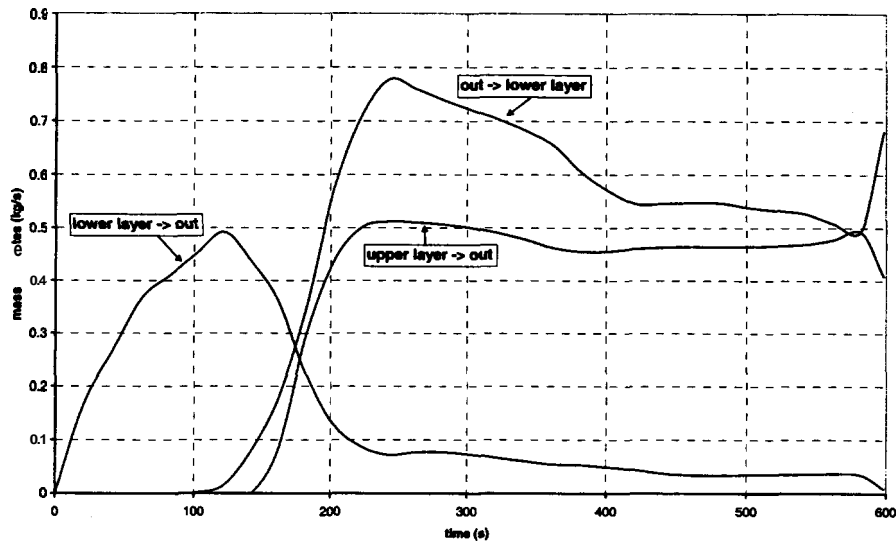


Figure 33: Mass flow rate through the door.

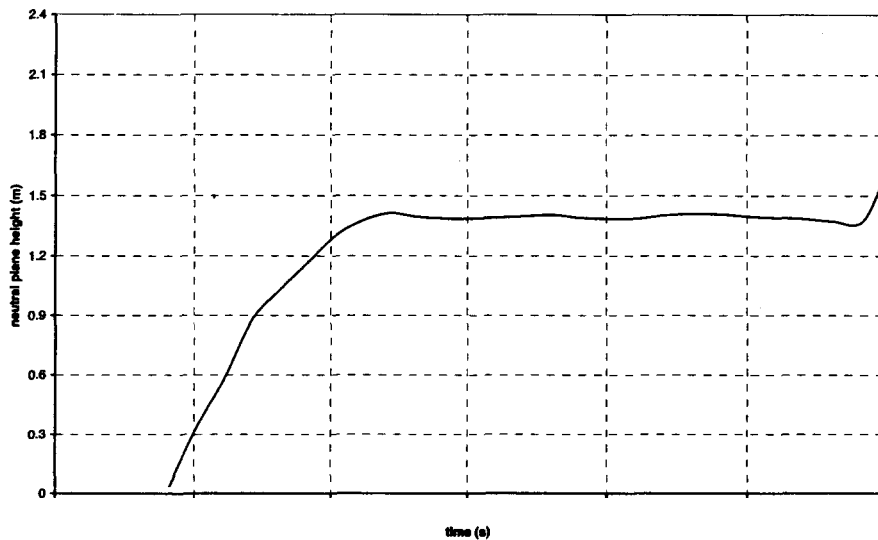


Figure 34: Neutral plane height.

Figure 33, Figure 34, Figure 35 and Figure 36 illustrate how mass flows take place through the door. For $t < 80$ s, the slight increase of the room temperature induces a flow from the lower layer of the room toward the outside. At $t \approx 80$ s a neutral plane occurs (Figure 34);

mass flow leaves and enters the lower layer of the room. For $t > 140$ s, the interface height in the room reaches the top of the door (Figure 35) ; mass flows leave the lower and upper layers of the room and enter the lower layer.

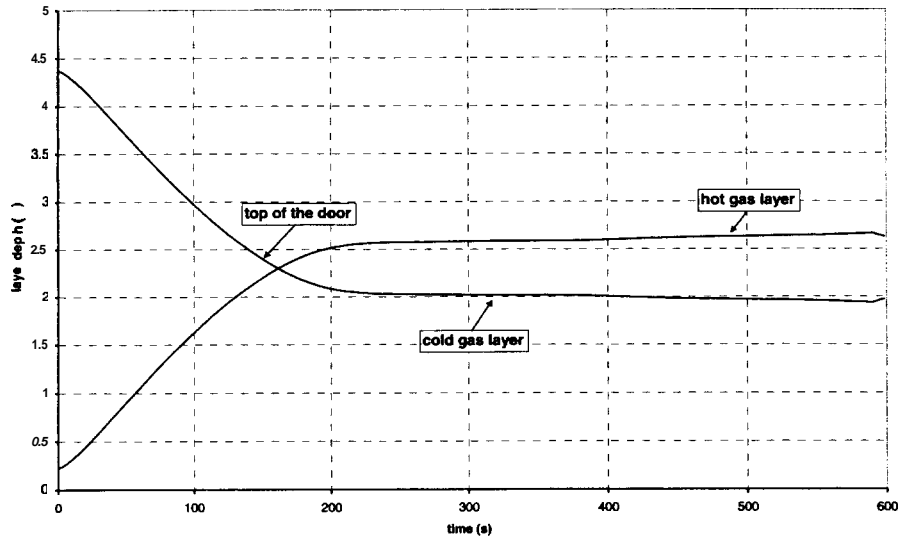


Figure 35: Depth of the upper and lower layers.

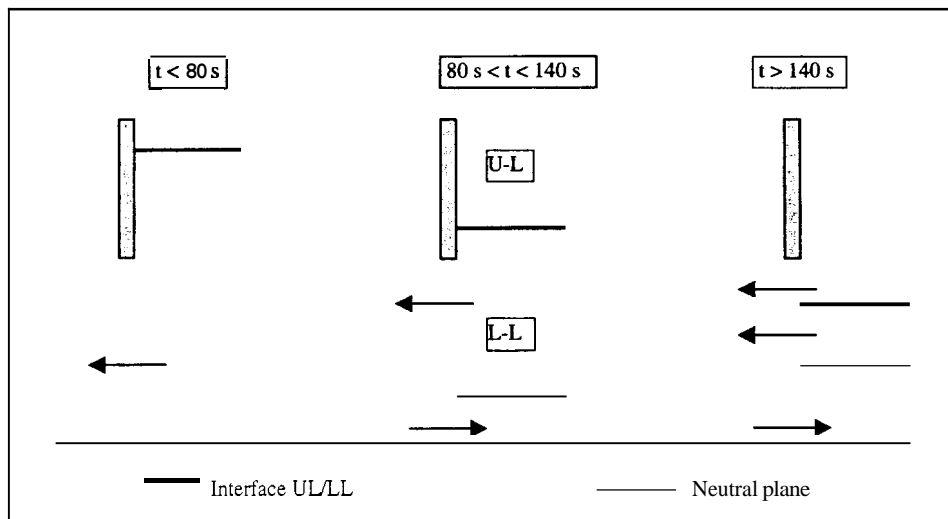


Figure 36: Mass flow rate through the door.

7.1.2 Case 5- Ventilation system on.

The Figure 37 and the Figure 38 show the mass flow rates through the air supply and exhaust vents. Since the density of the ambient air is 1.17 kg/m^3 , it corresponds exactly to a flowrate of 5 volume changes per hour.

The distribution of the flows between the upper and lower layers depends on the height of the interface. Before $t = 180 \text{ s}$, the interface height is higher than the top of the vent and all the flows enter and leave the lower layer. On the contrary, for $t = 480 \text{ s}$ the interface reaches the **bottom** of the vents and flows enter and leave the upper layer.

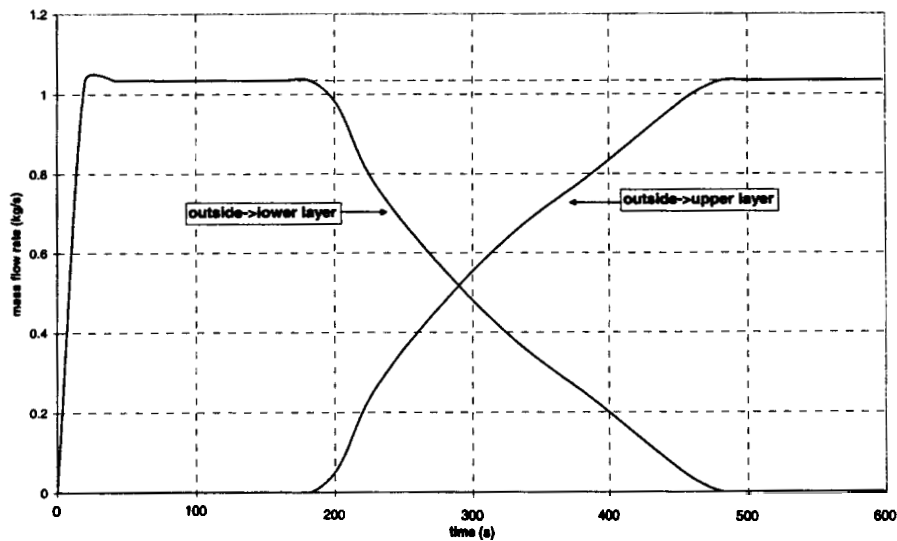


Figure 37: ~~Mass~~ flow rate through the supply vent.

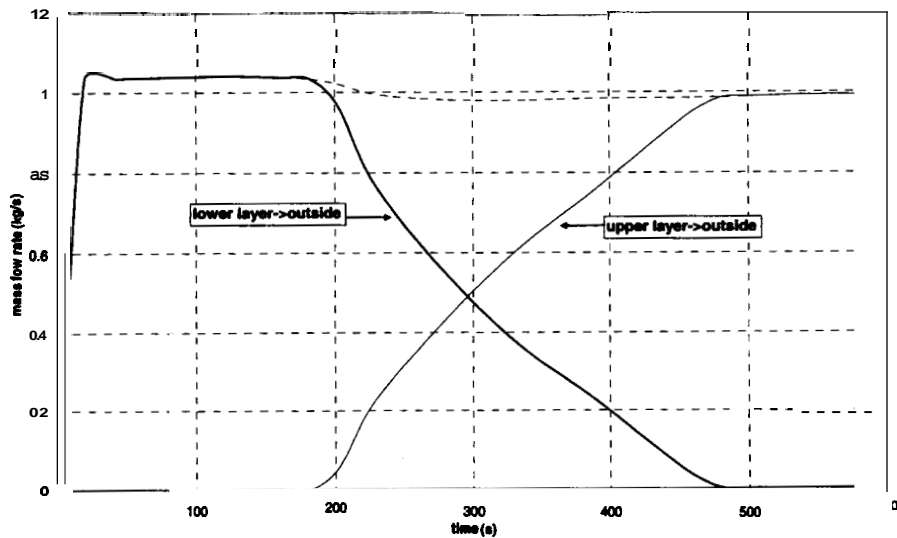


Figure 38: ~~Mass~~ flow rate through the exhaust vent.

7.2 Appendix 2.

7.2.1 Enclosed cases (1,2,3,4,5,6,7,8,13)

Combustion species concentration.

The Figure 39, Figure 40 and Figure 41 display the molar fraction of the chemical species in the upper layer for the base case and the cases 1 to 8 and 13.

As previously observed the fire duration does not exceed:

- 720 s for the cases 1,2,13,
- 556 s for the cases 3,4,5,
- 484 s for the cases 6,7,8.

From these times, the interface behave as a "solid" boundary that separates the upper and lower layers. No exchange between the layers occur and the molar fraction of the chemical species remain constant.

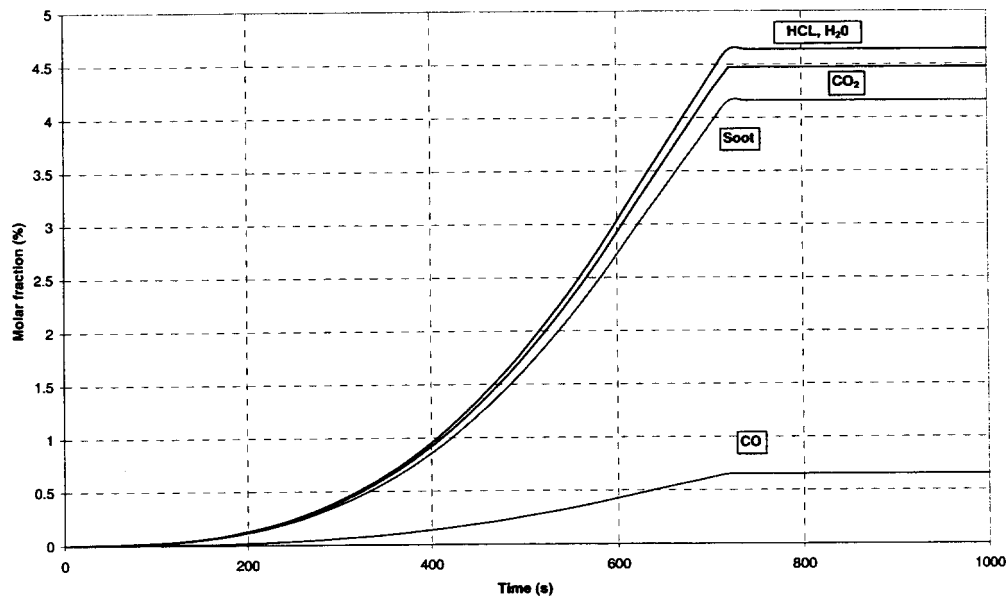


Figure 39 : Chemical species in the upper layer

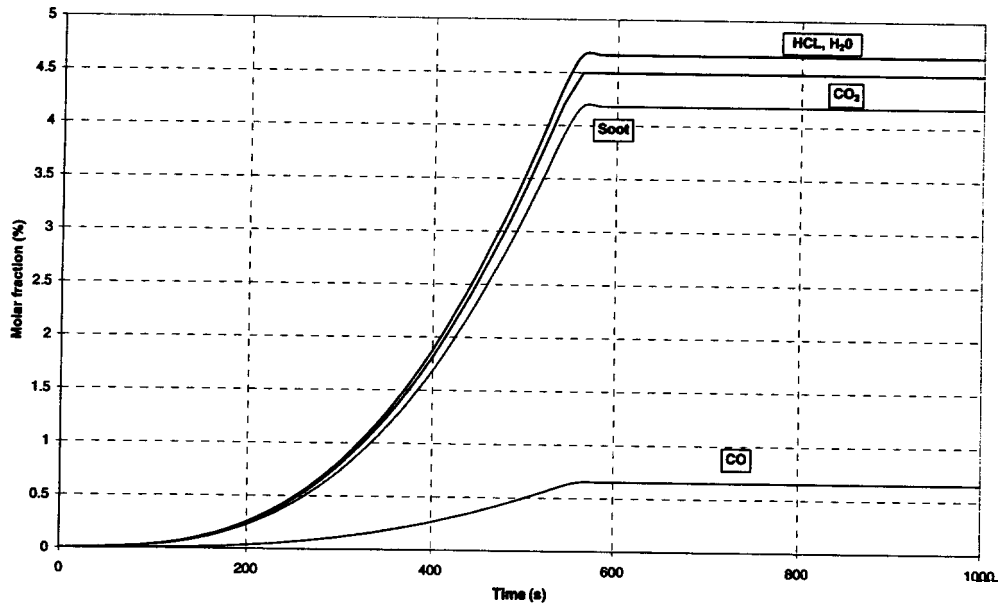


Figure 40 : Chemical species in the upper layer

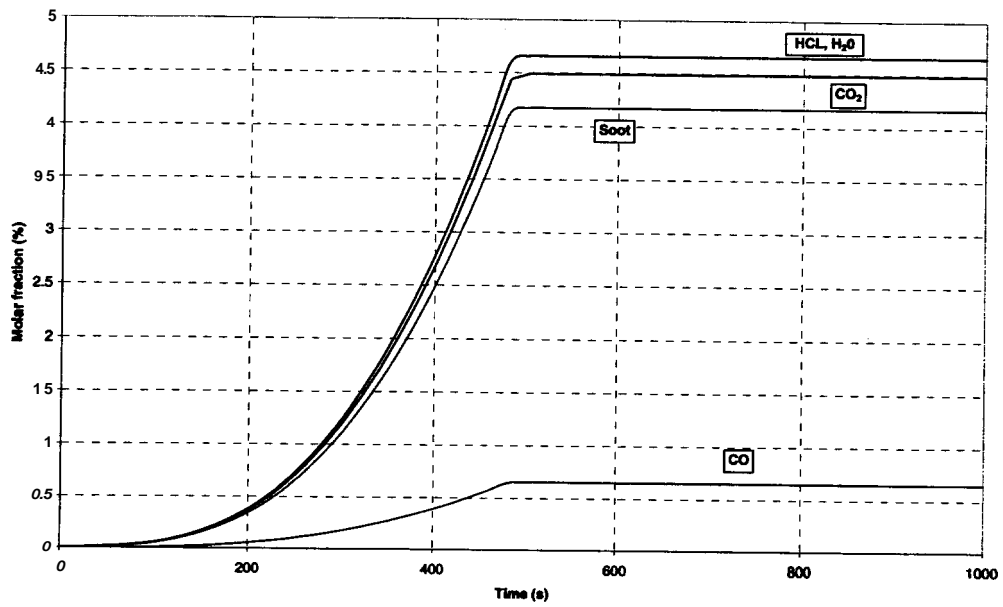


Figure 41 : Chemical species in the upper layer

Incident Radiant flux on the target (cabletray B)

The Figure 42 shows the incident radiant flux on the target. As previously explained, the profiles display a sudden slopes change corresponding to the time when the cable tray B enters in the upper layer.

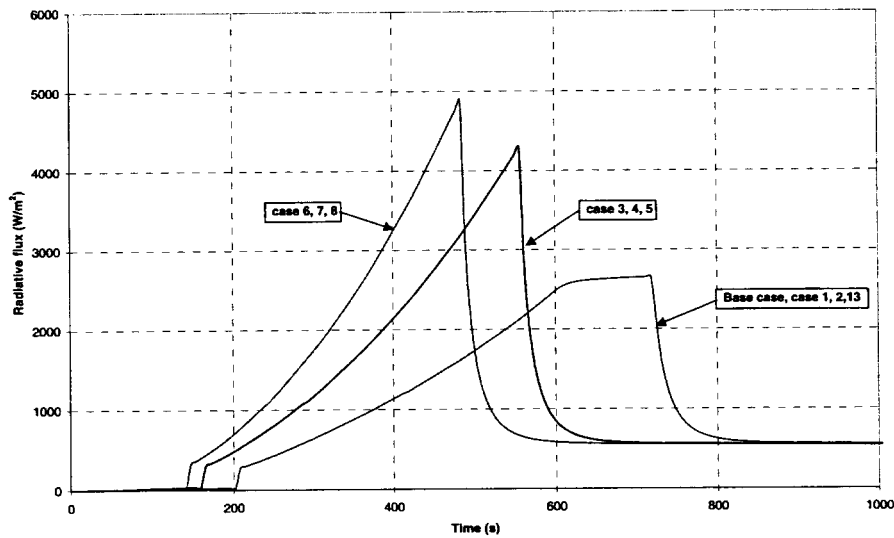


Figure 42 : Incident radiant flux on the target

7.2.2 Case 9.

The Figure 43 shows the molar fraction of the chemical species in the upper layer. As previously observed the fire duration does not exceed 720s and, from this time, the heights of the upper and lower layers are nearly constant. This explains the reason why no decrease of the molar fraction in the upper layer is observed.

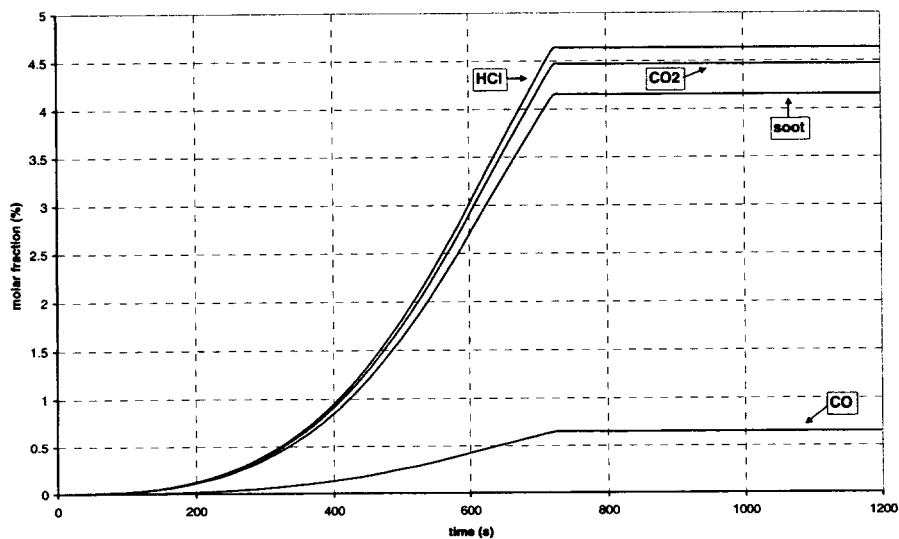


Figure 43: Chemical species in the upper layer.

The following figure is reported only to check that the ventilation system ensures a flowrate of 5 volume changes per hour in and out of the room.

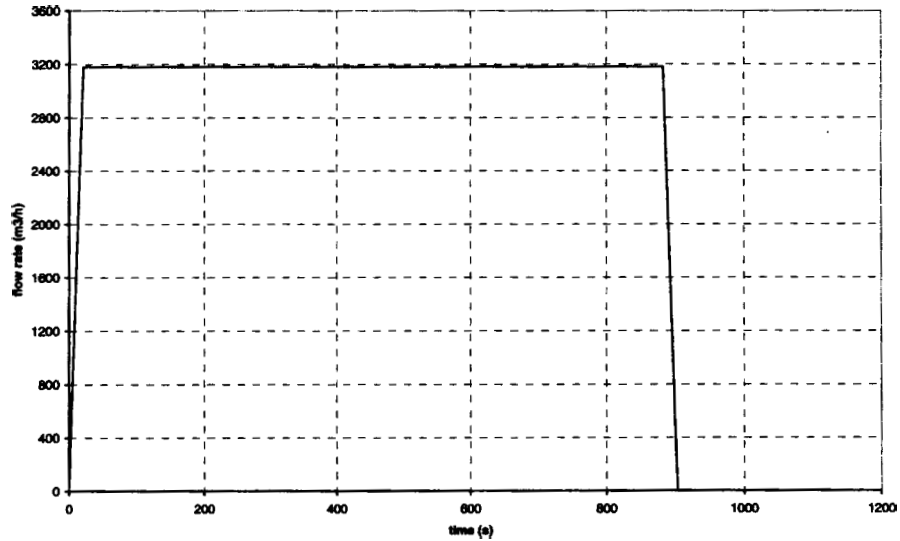


Figure 44: Flowrate in and out of the room.

7.2.3 Case 10.

The Figure 45 shows the molar fraction of the chemical species in the upper layer. As previously observed the fire duration does not exceed 720s and, from this time, the heights of the upper and lower layers are nearly constant (cf. Figure 31). This explains the reason why no decrease of the molar fraction in the upper layer is observed.

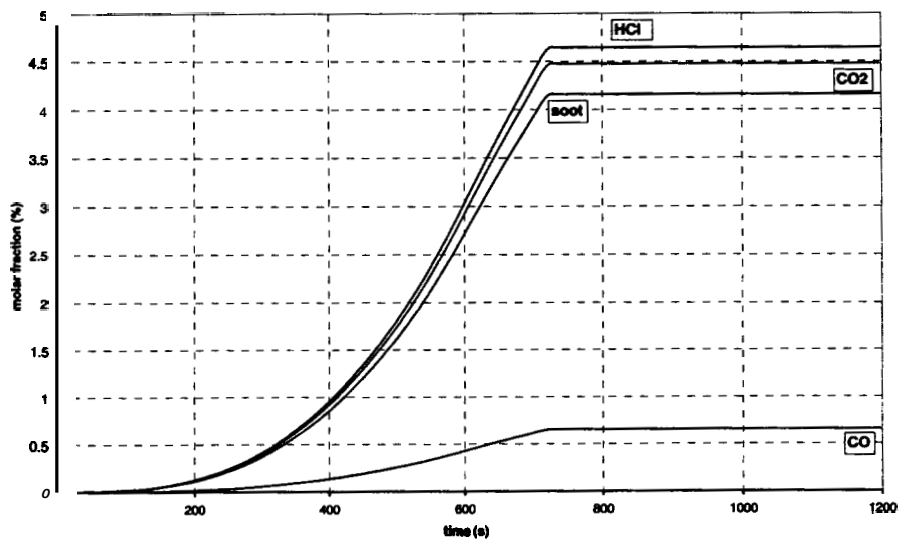


Figure 45: Chemical species in the upper layer.

The Figure 46 shows the mass flow rate through the door. Since the interface height never reaches the top of the door, only the lower layer is concerned with these flows.

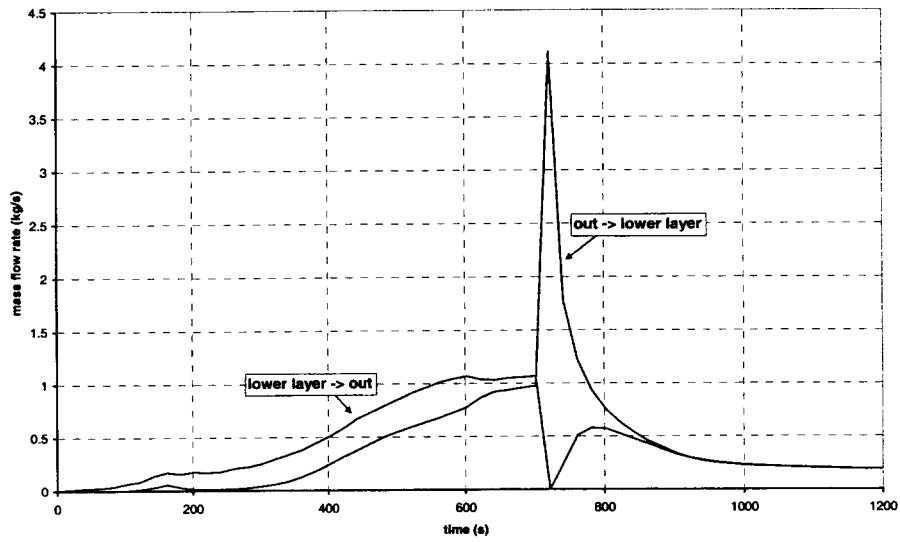


Figure 46: Flow rate through the door.

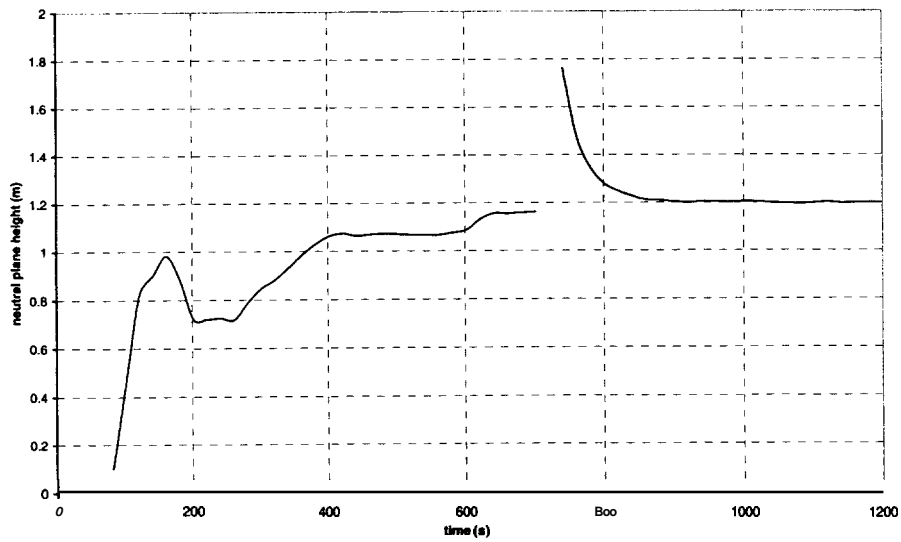


Figure 47: Neutral plane height.

